RSC Advances

ROYAL SOCIETY OF CHEMISTRY

www.rsc.org/advances

A table of contents entry

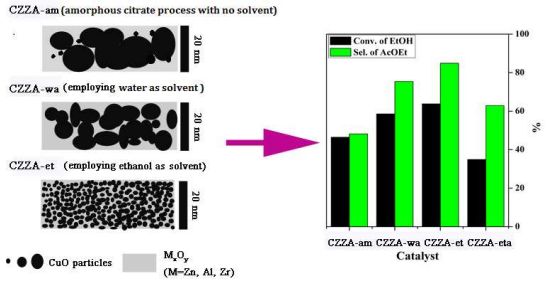

Solvent effect was vital and the Cu-Zn-Zr-Al-O prepared by modified citrate-complex process using ethanol performed best for ethanol conversion.

Synthesis of Cu-Zn-Zr-Al-O catalyst via a citrate complex route modified by different solvents and their dehydrogenation/hydrogenation performance

Jian Ding[a, b], Jiangang Chen[a,*]

a. State Key Laboratory of Coal Conversion, Shanxi Institute of Coal Chemistry, Chinese Academy of Sciences, Taiyuan 030001, Shanxi, PR China

b. University of Chinese Academy of Sciences, Beijing 100049, PR China

Abstract: The quaternary Cu-Zn-Zr-Al-O catalysts have been prepared by citrate-complex method using deionized water, ethanol, and ethyl acetate as solvents, respectively. The solvent with different polarity and solubility has a prominent influence on the reaction pathway(s) of the synthesis process. When using ethanol as solvent to prepare the catalysts, the selectivity and yield to ethyl acetate of 89.5 wt.% and 70.6 wt.%, which corresponds to 78.9 wt.% conversion of ethanol, is achieved. The one also shows good catalytic activity and stability (>120 h at 220 °C) in the conversion of ethanol contains 7 wt.% of water. Its remarkable performance is due to the existing of smaller CuO particles and their more uniform dispersion which is beneficial to form Cu-M_xO_y (M= Zn, Zr, Al) interfaces. Owed to that, the catalyst showing more strong basic sites associated with the high density of O^{2-} migrated from the interaction of Cu-M_xO_y, which is favorable for the dehydrogenative dimerization of ethanol to ethyl acetate; Furthermore, the moderate chemisorptions and desorption of H_2 makes it more favorable for ethanol dehydrogenation. It also proves to be

* Corresponding author. Tel.: +86 0351 4040290.
E-mail: chenjg@sxicc.ac.cn (J. G. Chen).

effective for a series of ethyl esters hydrogenations (*e.g.*, ethyl acetate, and diethyl oxalate), indicating a general promotion of these reactions by using ethanol as solvent to prepare the catalysts.

Key words: **Cu-Zn-Zr-Al-O catalyst; citric acid; solvent; ethanol dehydrogenation; ethyl esters hydrogenation.**

1. Introduction

The dehydrogenation/hydrogenation reactions are important facets of synthetic chemistry.[1] Taking this future large availability of bioethanol into account and for reducing greenhouse gas emissions that contribute to the global warming, the use of ethanol (EtOH) based on green chemistry as feedstock can be foreseen. Direct conversion of EtOH to ethyl acetate (AcOEt) through dehydrogenative dimerization with the liberation of H_2 is an attractive alternative and represents a simple, non corrosive and toxic, and economical process.[2-5] The reaction is a combination of dehydrogenation, which is preferred by low pressure, and dimerization, which is preferred by high pressure. In the case of ethanol (EtOH) dehydrogenation, the copper-based catalysts have been successfully employed because of their ability to maintain the C–C bond intact while dehydrogenating the CO–H bond. Nevertheless, there are two limitations of the Cu catalysts, including their inherent activity being lower than that of noble metals and irreversible deactivation mainly due to metal sintering.[6-8] To overcome these problems, such as Pd–Ag membrane reactor[9] and acceptorless dehydrogenation reactions[1, 10] have been recently developed, but these

systems require the extensive use of noble metals and hazardous substance such as phosphorus. From environmental and economic viewpoints, it is important to synthesize and develop new catalysts with a higher activity for the conversion of ethanol and better selectivity to ethyl acetate under mild conditions. Herein, we highlight the catalyst design for improving the activity and stability of Cu-based catalysts and the significant improvement in ethyl acetate selectivity based on the understanding of the reaction mechanism.

In a metal-oxide interface, one can have adsorption/reaction sites with complementary chemical properties, whereas truly bi-functional sites would be very difficult to create on the surface of a pure metal or alloy system.[11] Also, the metal-oxide interface determines the formation and stability of the intermediates present in the ethanol transformation process. Based on Bueno,[12, 13] a combination of the Cu^{1+}/Cu^{0} pair or Cu^{0} interfaced to ZrO_2 which may provide a synergism is needed to efficiently transform ethanol to ethyl acetate. In the case of the Cu-Zn-Zr-Al-O (CZZA) catalyst,[7, 14] the active site for the coupling of ethanol and aldehyde is at the mixed metal-oxide surface, not at the Cu metal surface. According to many reports,[15-17] by applying citrate complex method as an advanced wet chemical route, multicomponent catalysts have higher uniformity in particle size distribution and in combination, which exhibit higher synergistic interaction and cooperative catalysis than those prepared by the coprecipitation and impregnation. This technique is based mainly on the formation of metal chelate complexes in solution, followed by elimination of the solvent via drying, resulting in a gel that contains of the starting

cations. Then the organic fraction of this gel is removed by calcination, resulting in a very fine and reactive oxide powder. More encouragingly, chelating of solvated metal ions, as an exception, is governed by a relatively high contribution of entropy, due to the replacement of many solvent molecules around a metal ion by one chelating ligand.[18] Thanks to this behavior, most metal chelate complexes exhibit a relatively high stability. However, a few systematic studies have been made, taking the parameters of the first step, namely the citrate synthesis, into account. For example, the contribution of different solvents used in citrate complex method is seldom investigated. In the complexation process, specifically, not only does the solvent play an important role in the hydrolysis and condensation of metal ions, it also facilitates the nanoparticle growth of the synthesized materials.[19] Along this line, adsorption characteristics of the citrate-metal complex with the aid of solvents include the interaction between hydrogen-bonded citrate chains, surface coverage, and potential intermolecular interactions between citrate anions during nanoparticle growth are significantly important.[20] Furthermore, the stability of citrate complex in solution is influenced by the presence of short-range repulsive forces, *i.e.*, steric repulsion or electrostatic repulsion, which further affects nanoparticle growth.[20, 21] Therefore, the solvent used may affect not only the surface features but also the morphological characteristics of the synthesized materials.

To gain an insight into the effect of solvents on structural properties of Cu-Zn-Zr-Al-O catalyst in relation to their performance, we prepared CZZA catalysts by citrate-complex method employing deionized water, ethanol, and ethyl acetate as

solvents, respectively. The products formed during ethanol conversion on CZZA were AcOEt, acetaldehyde (AcH), diethyl ether (DEE), n-butanol (BOL), methyl ethyl ketone (MEK), crotonaldehyde (CROT), propanone (PrO), CO, CO_2, ethylene (ETE), and 1-butene (BTE), etc.. On the basis of our experiments and with respect to maximum catalytic activities of the CZZA catalysts, ethanol still seems to be the solvent of choice for the precursor synthesis. This strategy raises the prospect of using citrate-complex method employing ethanol as solvents to prepare catalysts for the efficient dehydrogenation of alcohols to functionalized carbonyls, and consequently contributes to the sustainable development of green chemistry. Based on the understanding in selective activation of C−O and O−H bonds, the catalysts can also be applied to hydrogenolysis reactions of ethyl esters which are the simple esters and good model compounds for studying the selective hydrogenation of C=O and C−O bonds to produce various chemicals.

2. Experimental

2.1. Catalyst preparation

All the reagent grade chemicals were supplied by Sinopharm Chemical Reagent Co., Ltd., China and used without further purification. Each quaternary catalyst CZZA sample was prepared by using $Cu(NO_3)_2 \cdot 3H_2O$, $Zn(NO_3)_2 \cdot 6H_2O$, $Zr(NO_3)_4 \cdot 5H_2O$, $Al(NO_3)_3 \cdot 9H_2O$, and citric acid monohydrate (CA). The method was essentially the similar procedure as for an amorphous citrate process introduced by Marcilly et al.,[16] where the deionized water,[15] ethanol, and ethyl acetate[22] were used as solvents. The

catalysts prepared were referred to as CZZA-x, where x = am, wa, et, and eta was the amorphous citrate process, and using water, ethanol, and ethyl acetate as solvents, respectively. Take the CZZA-et as an illustration, the mixed nitrates of Cu, Zn, Zr and Al with a desired molar ratio (12:1:4:2) were dissolved in ethanol. An alcoholic solution of CA (calculated as 1/3 mol CA/g eq. of each metal plus extra 5%) was dropped rapidly into the above mixed solution under vigorous stirring. Then, the mixture was evacuated under a pressure of 1.0 kPa at 60 ^{o}C. After the resulting solid had been heated in air at 170 ^{o}C for 2 h, it was calcined in air at 550 ^{o}C for 2 h to give a CZZA sample. Similarly, the CZZA-wa catalyst was prepared through mixing an aqueous solution of CA with nitrates of Cu, Zn, Zr and Al which were dissolved in deionized water; the CZZA-eta catalyst was prepared by adding an ethyl acetate solution of CA to nitrates of Cu, Zn, Zr and Al which were dissolved in ethyl acetate. While the preparation of CZZA-am catalyst was essentially the same procedure as for an amorphous citrate process, which was physical mixing CA with nitrates of Cu, Zn, Zr and Al without the aid of solvents. Equally, the hybrid catalysts (CZZA-m) were prepared by mechanical mixing ZnO, ZrO_2, and Al_2O_3 with CuO as base for comparison. In order to investigate the effects of the addition of ZnO and Al_2O_3 on structural evolution of CZZA-et, a sample of Cu/ZrO_2 (denoted as CZr-et) with the same Cu loading (*ca.* 54.2 wt.%) as CZZA catalysts was prepared by the citrate complex method employing ethanol as solvent.

Before the following utilization, the raw CZZA catalyst was tabulated, crushed and sieved to get particles with a size range of 0.18-0.25 mm.

2.2. Characterization of catalysts

The powder X-ray diffraction (XRD) patterns in the range of 5° to 85° at a scanning speed of 2° /min was collected on a DX-2700 with monochromatic Cu Kα radiation operating at 40 kV and 30 mA. Average particle sizes were calculated by the Scherer equation using the (111) peak position of CuO from XRD data [Eq. (1)].

$$d = \frac{K\lambda}{FW\cos\theta} \quad (1)$$

where K was a constant generally taken as unity (0.89); λ was the wavelength of the incident radiation (0.15405 nm); FW was the full width at half maximum and θ was the peak position.

Nitrogen physisorption isotherms were recorded by using a Mcromeritics TriStar II 3020 instrument. The samples were outgassed at room temperature for 24 h before the measurements. Specific surface area (S_{BET}) calculations were carried out by using conventional BET calculations. Pore volume (V_{pore}) and average pore diameter (d_p) was deduced by using BJH pore analysis based on the desorption branch of the nitrogen adsorption/desorption isotherm. The surface morphology and the particle size were observed by transmission electron micrography. The TEM measurements were performed with a JEM-2100F microscope operating at 200 kV. Samples for TEM were prepared by depositing a drop of an ultrasonically dispersed solution onto a standard amorphous carbon-coated copper grid.

The reducibility of the catalysts was studied by H_2 temperature-programmed reduction (H_2-TPR) on a homemade apparatus.[23] A flow of 5% H_2 /N_2 (50 mL/min)

was passed through the 20 mg of sample with a ramping rate of 10 °C min^{-1} to a final temperature of 600 °C. The effluent gas formed during the TPR experiment was passed through a molecular sieve trap to remove the water. In the meanwhile, the hydrogen consumed was monitored continuously by a thermal conductivity detector (TCD). Calibrating of the instrument by the hydrogen consumed was carried out with 20 mg standard samples of CuO (Aldrich). The dispersion and specific surface area of metallic copper (D_{Cu} and S_{Cu}) were measured by one-pulse N_2O oxidation at 50 °C using the procedure described by Van Der Grift et al..[24, 25] The calculation was based on the total amount of N_2O consumption with 1.46×10^{19} copper atoms per m^2. For more details, see the Electronic Supplementary Information. The activation and desorption properties of hydrogen were tested by temperature-programmed desorption of adsorbed H_2 (H_2-TPD) using the same apparatus employed by TPR experiment. Prior to H_2 adsorption, the sample (120 mg) was reduced in a H_2 (50 mL /min) gas flow at 250 °C for 4 h. Then the sample was pretreated under Ar flow (50 mL/min) at 350 °C for 1 h to sweep the surface of the reduced catalyst. After cooled to room temperature by Ar flushing, the sample was exposed to H_2 (50 mL /min) for 1 h and heated to 600 °C by steps of 15 °C /min. The effluent formed during the experiment was purified by silica gel desiccant and 5A molecular sieve to eliminate water and other substances produced in the test, and subsequently monitored by TCD. H_2O-TPD measurement was carried out to investigate the adsorption/desorption of water on the catalysts. Before any measurements, all samples were in situ saturated with water after reduced in H_2 (50 mL /min) for 4 h. The temperature was subsequently ramped

from 50 °C to 700 °C with a linear rate of 15 °C /min under He flow (30 mL/min), and the tail gas was continuously monitored on stream by the TCD. Temperature-programmed desorption of adsorbed CO_2 (CO_2-TPD) on the reduced catalysts was analyzed using a quadrupole mass spectrometer (HIDEN, Hpr-20; Pfeiffer Vacuum Technology AG) equipped with the same apparatus employed by TPR experiment. Prior to CO_2 adsorption, the sample (200 mg) was reduced in a H_2 (30 mL /min) gas flow at 250 °C for 4 h. After reduction, the sample was swept at 350 °C for 1 h and subsequently cooled to room temperature by a He gas flow (50 mL /min). Then several CO_2 pulses (1.2 mL CO_2 of one pulse) were introduced to the sample to obtain a saturated adsorption of CO_2. The sample was purged by He for 1 h at 100 °C in order to eliminate the physical adsorbed CO_2, then the sample was heated to 650 °C by 15 °C /min in He and the effluent was continuously monitored by the mass spectrometer. Mass number used were 44 for CO_2 species.

The purity of the gases N_2, Ar, He, N_2O, CO_2, and H_2 were greater than 99.99%, and all of them were pretreated by silica gel desiccant, 5A molecular sieve and some of them were deoxygenated by silver molecular sieve before using.

2.3. Catalytic activity tests

Evaluations were conducted on a stainless steel fix-bed reactor (9.8-mm i. d.). The catalyst (2 g) placed between two layers of quartz sands was reduced in a stream of diluted hydrogen (10% H_2 in N_2) at 250 °C under atmospheric pressure for 16 h with a flow rate of 30 mL/min. Then the catalyst was heated to the desired reaction

temperature by steps of 2 ^{o}C /min. The liquid reactant was injected by double-plunger pump enabling a tunable liquid hourly space velocity (LHSV). After vaporized by a pre-heater, the vapor mixed with the N_2 or H_2. Details of the reaction conditions were presented below each result. The condensable obtained products were collected in a trap and analyzed by gas chromatography (Shimadzu GC-14C) using a capillary column (19091n-213, HP-INNOWAX, 0.25 mm × 30 m) with FID as the detector and a packed column (TDX-101) with TCD as the detector. The gas products were periodically analyzed by online gas chromatographs (Shanghai Haixin GC-950) with a packed column filled with carbon molecular sieve). The products were determined quantitatively by calibrated area normalization. Meanwhile, conversion and selectivity were based on the mass basis products (wt.%) and calculated by the equations in Electronic Supplementary Information.

1 **Table 1** Physicochemical properties and catalytic performance of the CZZA-x catalysts

Catalyst	D_{Cu} (%)[a]	S_{Cu} (m^2/g_{cat})[a]	d_p (nm)[a]	S_{BET} (m^2/g_{cat})[b]	V_{pore} (m^3/g_{cat})[b]	(S_I/S_{II})[c]	Conversion (wt.%)[d]	Sel. of AcOEt (wt.%)[d, e]	Yiel. of AcOEt (wt.%)[d]	Yiel. of H_2 (wt.%)[d]
CZZA-am	6.5	24.6	15.4	71.2	0.095	0.28	46.5	58.2	27.1	1.9
CZZA-wa	11.9	41.5	8.4	68.6	0.079	0.45	58.6	70.4	41.2	2.6
CZZA-et	14.1	49.2	7.1	84.7	0.080	0.65	63.8	84.9	54.2	3.2
CZZA-eta	8.4	29.3	11.9	65.1	0.084	0.31	44.9	52.9	23.8	1.9

2 [a] Cu dispersion and surface area of Cu^0 were determined by N_2O titration. [b] Measured by BET method for the calcined sample. [c] H_2O-TPD peak area ratios of the

3 lower temperature desorption peak I to the higher temperature desorption peak II of CZZA-x. [d] Reaction conditions: P = 0.1 MPa, LHSV = 1.0 mL/(g_{cat} ·h), and T =

4 220 ^oC. [e] Other condensable byproducts (*e.g.*, AcH, MEK, CROT, PrO, and H_2O, etc.) and gaseous products (*e.g.*, CH_4, C_2H_6, CO, and CO_2, etc.) were also formed.

5

6

3. Results and Discussion

3.1 Textural and structural properties

The X-ray diffractograms of all prepared catalysts are shown in Fig. 1. All samples exhibited main sharp peaks at = 32.6, 35.6, 38.6, 48.8, 53.6, 58.3, 61.6, 66.4, 68.1, 72.3 and 75.1° corresponding to a crystalline CuO phase with tenorite structure (JCPDS 481548). Because there were no peaks obtained corresponding to ZnO and Al_2O_3, indicating that the dispersion of them was more uniform and they were present in highly disordered or amorphous states.[26, 27] Apparently there was a decrease of the peak intensity of copper species (Fig. 1). The average CuO crystallite sizes, which were estimated by Scherrer's equation, were 19.8, 14.1, 10.9, and 8.6 nm for CZZA-eta, CZZA-am, CZZA-wa, and CZZA-et, respectively. Table 1 shows dispersion and surface area of Cu^0, surface area, pore volume and average pore diameter values for the CZZA catalysts. Although the samples did not show much difference in the V_p and d_p, the S_{BET} and S_{Cu} determined by N_2O titration method (Fig. 1S) were different, and the dispersion of copper species followed the sequence of CZZA-et>CZZA-wa>CZZA-eta>CZZA-am. Among the samples, CZZA-et displayed the highest surface area (84.7 m^2/g_{cat}) and copper surface areas (49.2 m^2/g_{cat}). It was probable that the increase in Cu surface areas were caused by the decrease in the particle size of CuO species, as shown in the XRD patterns of CZZA-et (Fig. 1). Based on the data above, we concluded that the CuO particle sizes in the CZZA-et became the smallest and the dispersion of Cu species was more uniform, indicating

that the solvents used in the preparation process had a great influence on the dispersion of the copper species.

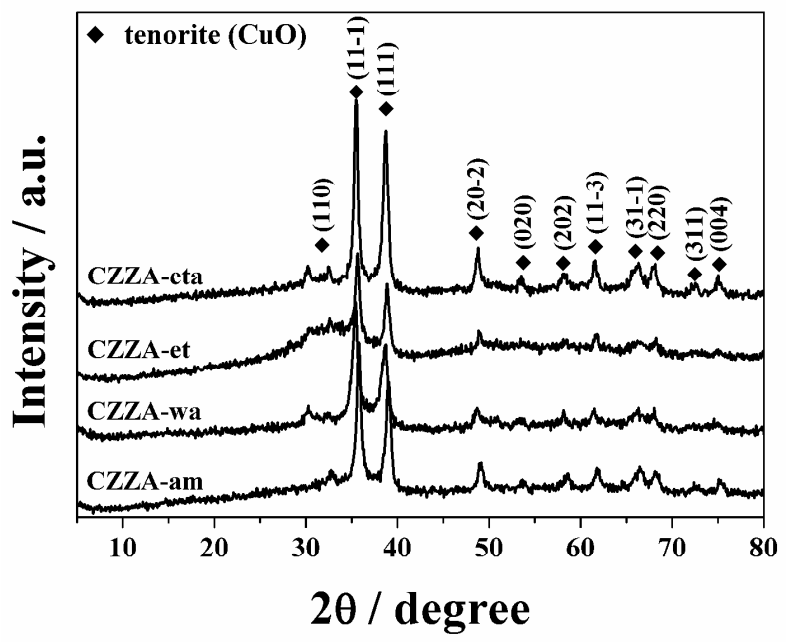

Fig. 1 XRD patterns of calcined CZZA samples prepared by citrate-complex method.

Fig. 2a-c compares TEM images of the calcined CZZA-x catalysts. These showed that the catalysts consisted of clusters of interconnected particle with sizes of 5–50 nm (Fig. S2e). For CZZA-am and CZZA-wa (see Fig. 2a and 2b), the CuO particles were agglomerated into clusters larger than 15 nm in size, which also verified by XRD. The morphology of the two calcined catalysts clearly demonstrated that the CZZA-am and CZZA-wa catalyst often appeared in larger agglomerates than the CZZA-et which resulted in the lower BET surface area and dispersion of Cu^0 (Table 1). Apparently, the corresponding dispersion of copper species increased by employing ethanol as solvent could be directly observed from the TEM image of the CZZA-et sample (Fig. 2c). Also the image for the CZZA-et sample showed little obvious evidence of bulk copper species condensed on the substrate M_xO_y (M= Zn, Zr,

Al), which further confirmed that the copper species were uniformly dispersed in the CZZA-et after the synthesis process and the following high-temperature thermal treatment. As can be seen in Fig. S2, contrary to the agglomerated particles in CZZA-wa, the magnified TEM images of CZZA-et show small particles of narrow dispersity which embedded in an amorphous matrix, which are, most probably formed from the substrate of M_xO_y. Furthermore, the higher agglomeration and thus higher density of the particles enables additional confirmation of the crystallinity of the CZZA-wa using selected area electron diffraction (SAED) (Fig. S2e). Also, the amorphous structure of M_xO_y, the small and even of CuO can be further confirmed by a successive diffraction halo in an attached SAED image for CZZA-et (Fig. S2c). Generally speaking, this was because small CuO particles adhered to the surface of M_xO_y, hence the sintering of copper particles was obstructed, as seen from schematic illustration (Fig. 2d). This was in agreement with the results from XRD and metallic copper surface area measurement (Table 1 and Fig. 1S). However, the metallic Cu particle size of CZZA-wa catalyst observed by TEM was larger than the crystallite size derived from XRD and N_2O titration indicating the polycrystalline nature of the metallic Cu particles in CZZA-wa than that of other samples. This could probably be connected with the water's contribution, which was convenient for the intimate contacting of Cu species in the precursors by building strong hydrogen-bonded networks, and then affected the sintering behavior in the following high-temperature thermal treatment, for example, forming the agglomeration or polycrystalline of CuO. Thus, the nanostructure was not distinctive in the images of TEM. In a word, the big

difference of the active copper surface area among CZZA-x may originate from the differences in copper particle size and dispersion. Moreover, the increase in Cu^0 surface area and Cu-M_xO_y interfaces is assumed to be partially responsible for the improvement of dehydrogenation and dimerization activity.

The TEM images of the Cu/ZrO_2 catalysts are shown in Fig. 2(e). The morphology of the CZr-et and CZZA-et catalysts clearly demonstrated that the binary catalyst consisted of small particles of similar shape, while often appeared in larger agglomerates, than the quaternary catalyst did. The aggregation of CuO nanoparticles in CZZA-et was not significant as CZr-et. The combination of Al and Zn oxides with Zr oxide had been described as preventive elements for sintering of Cu crystallites and therefore was considered as structural promoter and as alternative support.[27] Moreover, the introduction of ZnO and Al_2O_3 effectively stabilized copper and prevented crystallite growth. As shown in Fig. 2(c), it was clear that CZZA-et catalysts exhibited better resistance to Cu/CuO particle growth upon calcination than the binary CZ-et catalyst. The results showed that the addition of ZnO and Al_2O_3 had a significant influence on the particle size distribution and the structure of the catalyst with the aid of ethanol as solvents. In addition, based on "X-ray amorphous" features for CZZA-et, the zinc, zirconium, and aluminum phases were present in an amorphous-like state in the quaternary catalysts.

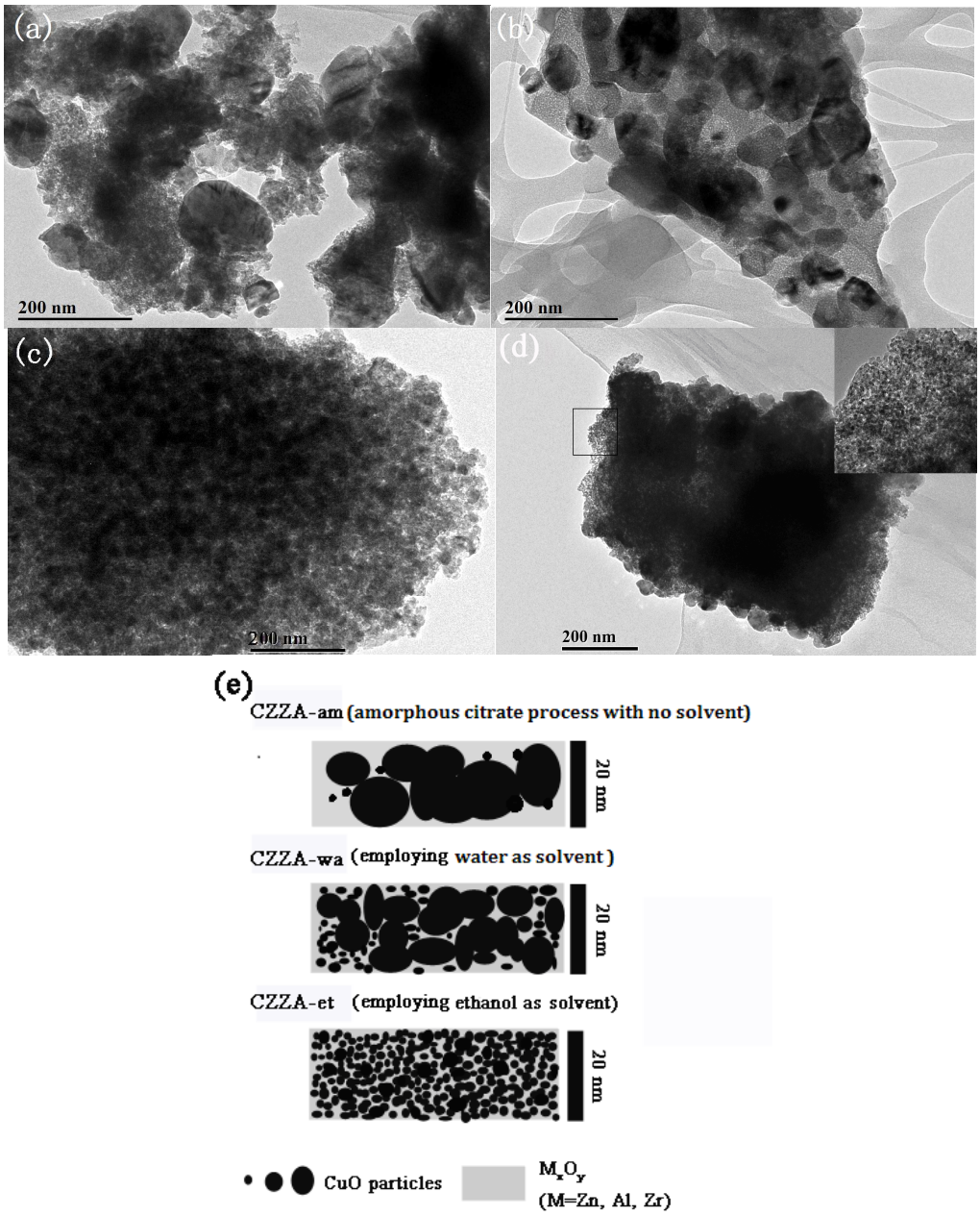

Fig. 2 TEM images of the calcined quaternary catalysts (a) CZZA-am; (b) CZZA-wa; (c) CZZA-et and (d) the calcined binary catalyst Cu/ZrO_2; (e) schematic illustration of the structural evolution of the nanostructured CZZA catalyst as a function of solvents.

3.2 H_2-TPR analysis

Fig. 3a compares the H_2–TPR profiles for CuO, and the four prepared CZZA-x catalysts. All of the samples displayed reduction profiles characterized by a main peak

with a maximum between 160 and 270 °C, well below that of the standard bulk CuO (*ca.* 285 °C), suggesting the presence of a copper-oxides interaction in the present samples, which facilitated the reduction of copper oxides. In fact, the peak was sharper and much more symmetrical for CZZA-am, CZZA-wa, and CZZA-eta. While the profile of CZZA-et displayed a weak reduction peak centered at *ca.* 162 °C which was lower than that of the sharp one. Fig. 3b shows typical TPR profiles before and after N_2O oxidation for CZZA-et. The peak area of the first TPR profile (TPR 1) corresponded to all CuO in the sample, and that of the second TPR (TPR 2) corresponded to Cu_2O produced by N_2O oxidation. In fact, the TPR peak was at around 130 °C for surface Cu^+ to Cu^0 compounds and 170 °C for small CuO particles to Cu^0 in Fig. 3b. As stated, the peak took place at 192 °C for CZZA-et was unlikely to be caused by the reduction of Cu^{1+}, but rather, by CuO particles with small sizes.[28] As is known, the more facile reduction-oxidation of Cu species in the small CuO particles was presumably due to a higher degree of surface defective dominant features which meant a poor crystallinity with plenty of weakly bonded surface oxygen ions and higher surface area exposed to H_2; whereas the large crystallites would appear in the TPR as species reducible at a higher temperature because of the diffusion hindrance on the reduction process and/or their relatively lower surface area exposed to H_2.[27, 29] In this case, the reducing temperature in the profiles of TPR can be used to reflect the size of the Cu particles, e.g., CuO phase with a low reduction temperature denoted a small particle size.[30] Secondly, according to Behrens et al.,[31] the crystalline and pure CuO species were easier to be reduced than the highly

dispersed CuO in amorphous materials as a result of diffusion effects and the strong interactions between Cu species and M_xO_y. The higher reduction temperature of second peak than the former peak for CZZA-et indicated the presence of highly dispersed CuO species embedded into the supports of M_xO_y. Moreover, interactions with supports can decrease the rate of CuO reduction.[32] The consumption of H_2 for CZZA-et was lower than that of CZZA-am and CZZA-wa which further confirmed that highly dispersed CuO particles strongly interacted with the M_xO_y thus decreasing the rate of CuO reduction. In a word, we proposed that there were two reducible copper species in CZZA-et catalysts. One was represented by small crystalline CuO which were finely dispersed, they reduced at lower temperature (peak I); another was possibly represented by highly dispersed CuO strongly interacting with the M_xO_y supports, they reduced at higher temperature (peak II). Deconvolution of the two TPR peaks indicated that the amounts of small CuO and Cu-M_xO_y were *ca.* 10% and 90%, respectively. Interestingly, the two-peak H_2–TPR profile of CZZA-et was consistent with a phenomenon discussed in detail in H_2–TPD and elsewhere[33] regarding the generation of sites for medium absorption of H_2.[34] More details about it will be given below. On the other hand, the reduction of CuO strongly interacted with the support, although existed in other three samples, can be partially covered up by the reduction of large CuO crystallites. As consequence, the reduction temperature of CZZA-x catalysts increased and followed the order of CZZA-et < CZZA-wa < CZZA-am < CZZA-eta. Thus, the increasing reduction temperature in the profiles of TPR indicated the increasing size of CuO particles and/or possibly a strong interaction between

copper and supports, which in accordance with XRD and TEM results. Furthermore, it should be noted that the TPR measurement can be explained partially in terms of copper dispersion, especially for the sample containing zirconia because of the introduction of ZrO_2 in the sample facilitating the reduction of CuO.[27, 29] The CZZA-et catalyst displayed the lowest reduction temperature that both the weak reduction peak centered at *ca.* 162 °C and main peak appeared at approximately 220 °C. This indicated the smaller CuO particles and hence, a higher dispersion than that of other samples. These results correlated well with the metallic copper surface area measurements and XRD results.

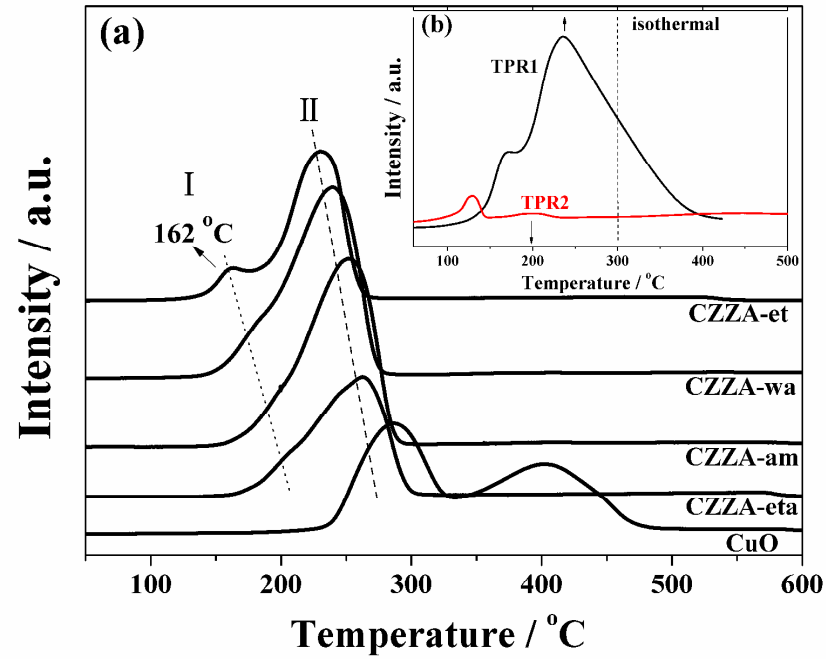

Fig. 3 a: TPR profiles of the CZZA catalyst prepared by citrate-complex method and bulk CuO; b: reduction profiles of CZZA-et catalyst before and after N_2O oxidation at 50 °C.

3.3 H_2-TPD analysis

The H_2-TPD profiles of the reduced CZZA-x catalysts are shown in Fig. 4. Two

obvious H_2 desorption peaks (centered at 152 and 460 ^oC) and a slight peak (centered at 580 ^oC) appeared in the whole T range over for all the samples, which were similar at temperature, but differing greatly in the size. According to those published works in this area,[35-37] the resolved peak at low temperature (120–240 ^oC) could be ascribable to the hydrogen moderately adsorbed on Cu (hydrogen on surface Cu sites). While a much broader signal in the range of 350–530 ^oC monitored the desorption of hydrogen from the split H–H on the surface of Zn–Al–Zr-O oxides or CuHx which denoted as hydrogen strongly adsorbed on Cu, and the weak peak after 540 ^oC would be due to oxidation of the metal by support protons, respectively. Thus, H_2-TPD pattern of CZZA-x catalysts span a wide range of temperature (50-670 ^oC) was diagnostic of different adsorption states of hydrogen species across the catalyst structure (Fig. 4). At the first stage (corresponding to peak I), sites were probably being formed that had a high efficiency for the adsorption of H_2 and thus produced moderately adsorbed hydrogen on surface Cu sites.[36, 38] Apparently, these peaks enhanced in CZZA-et and CZZA-wa, while lowered in CZZA-eta and CZZA-am because of the decreasing of small CuO particles which were liable to be transformed to Cu^0. The high-temperature peak (corresponding to peak II, denoted as hydrogen strongly adsorbed on catalysts) was attributed to the generation of sites for facile H_2 dissociation which was helpful to form CuHx. The catalytic activities test for CZZA-am indicated that the one had a strengthening of peak II and weakening of peak I in the TPD profile showed a relatively low catalytic activities for ethanol dehydrogenation (46.5 wt.% conversion of ethanol and 58.2 wt.% selectivity to AcOEt). The same phenomenon was observed

over CZZA-m (16.5 wt.% conversion of ethanol and 26.5 wt.% selectivity to AcOEt, data not shown here) which only displayed surface sites for H_2 dissociation. For CZZA-et which showed the best catalytic activities (*ca.* 64 wt.% conversion of ethanol), had the highest TPD peak area of the lower temperature peak I. Therefore, the catalysts` dehydrogenation activity decreased with increasing amounts of strong desorption of H_2. These results suggested that hydrogen activation driven by the adsorption-desorption of H_2 for CZZA-x markedly contributed to the H_2 activation ability and these enhanced H_2 activation ability (by the way, the desorption of H atom would be very difficult) may impair its activity for dehydrogenation of ethanol. Qualitatively, the key to increase catalytic activity derived from the balance between the number of active sites and the ease of product desorption. In other words, the moderate chemisorptions and desorption of H_2 avoided competitive adsorption of H and ethanol or acetaldehyde on metallic active sites, meanwhile, recombination of H and ethoxide to yield ethanol again.[12, 13]

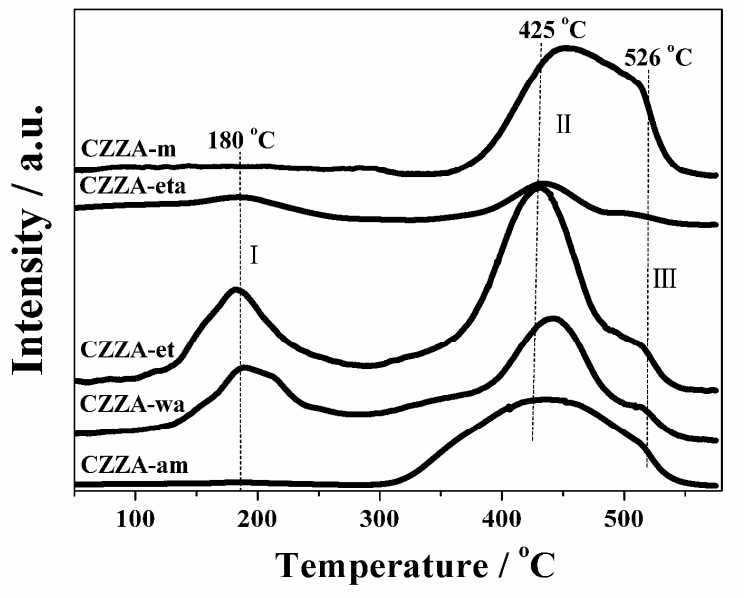

Fig. 4 H_2-TPD profiles of the reduced CZZA-x catalysts.

3.4 H_2O-TPD analysis

The H_2O-TPD profiles of the CZZA-x catalysts are shown in Fig. 5. There were two obvious H_2O desorption peaks (centered at 152 and 382 ^oC) appeared over CZZA-x catalysts. Both of them were similar at temperature, but differing greatly in the size. Clearly, the TPD peak area of the lower temperature peak I enhanced in CZZA-et and lowered in CZZA-eta indicated that there were more active sites for adsorption/desorption of H_2O under reaction temperature. The much broader peak II denoted as H_2O strongly adsorbed on Cu. Obviously, the strong adsorption of H_2O competed with ethanol or acetaldehyde on the surface of CZZA-x catalysts and led to the hindering of ethanol conversion. Table 1 compares TPD peak area ratios of the peak I to the peak II for the CZZA-x catalysts. Analyses indicated that the catalyst had a high S_I/S_{II} ratio showed a relatively high desorption activity for water on the catalyst, meanwhile, afforded more active sites for the adsorption of ethanol. Based on above, one can suppose that CZZA-et would show better catalytic activities in conversion of hydrous ethanol because the substantial desorption of H_2O avoided competitive adsorption of H_2O and ethanol or acetaldehyde on metallic active sites under reaction temperature.

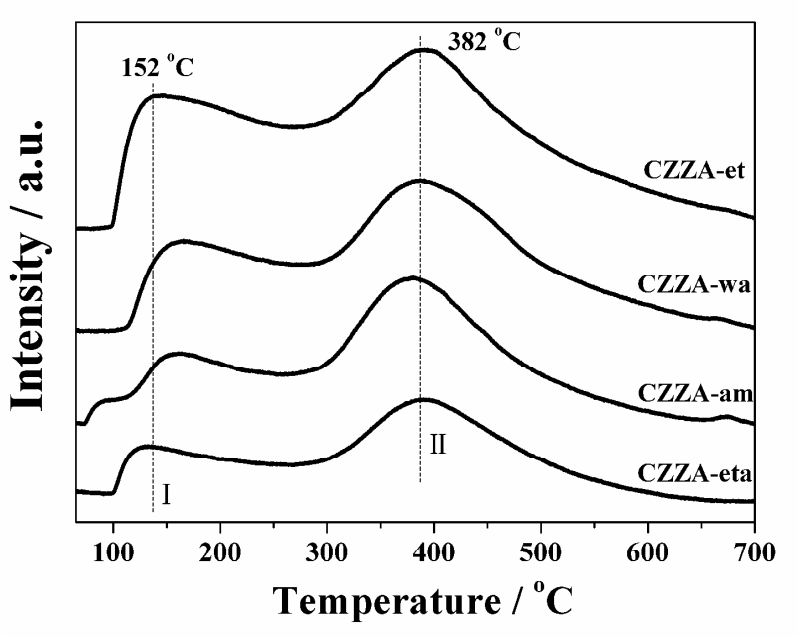

Fig. 5 H_2O-TPD profiles of the reduced CZZA-x catalysts.

3.5 CO_2-TPD analysis

As known to all, zirconia possessed surface Lewis basic sites which were able to adsorb CO_2, while the ZnO enhanced the affinity of the system to CO_2.[36] Moreover, the combination of Al oxide with Zn and Zr oxides probably reduced the acidity of alumina.[27] CO_2-TPD profiles of CZZA samples are shown in Fig. 6. As it can be verified, these samples showed different profiles regarding their interaction with CO_2. Several obvious CO_2 desorption peaks (at 150–180 and 320–500 °C) appeared in the whole T range over. The weak basic sites were related to a curve which showed a maximum at a temperature *ca.* 180 °C; the ones between 350 and 500 °C, were strong basic sites; and finally, the peaks above 550 °C, were due to the release of CO_2 from support.[39] Thus, the CO_2-TPD profile of CZZA-x disclosed a clear concentration of varied basic sites on surface (Fig. 6). As it can be observed, CZZA-et showed the largest peak for strong basic sites followed by CZZA-wa, and CZZA-am. While there

were no distinct peaks of desorption of CO_2 for CZZA-eta, instead of a broad and lower peak with maximum between 350 and 520 ^oC, similar in qualitative (curves in Fig. 6) for CZZA-et; the same to CZZA-am was that a broaden peak of desorption of CO_2 with maximum between 400 and 520 ^oC. Therefore, the CO_2-TPD profiles indicated an increasing contribution of stronger basic sites associated with the interaction between Cu and M_xO_y. In other words, the high density of basic sites associated with the oxygen sites originated from the oxygen-rich interface at Cu–M_xO_y by oxygen diffusion. This implied that the location of O preferred a high coordination environment on neutral Cu system where the surface electron density was high, in line with the strong ionic bonding character of O and Cu.[32] As was verified that acetaldehyde produced on the dehydrogenation catalyst migrated towards the oxides and reacted with the ethoxide species which were generated by the oxide basic sites. The resulting hemiacetal was dehydrogenated and the ethyl acetate obtained was desorbed. Clearly, oxides with strong basic sites generated the most effective systems than weak ones for the ethyl acetate synthesis**.** [14, 40] For all the samples used in these experiments, CZZA-et showed the best catalytic activities (Table 1). Actually, when CZZA-eta was employed, the lower selectivity to ethyl acetate was observed than those of CZZA-et (52.9 wt.% vs. 84.9 wt.%). The low selectivity to ethyl acetate observed from the other ones might be associated with the low density of the strong basic sites. Above all, we can conclude that the basic sites on the CZZA-et interacted strongly with Cu nanoparticles and formed Cu–M_xO_y, generating a catalytically active nanoenvironment for the reaction coupling between

alcohol dehydrogenation and dimerization.[41] That meant a synergism of metal Cu dehydrogenation and oxide basic sites dimerization which provided the metal/oxide interface on the functionality of Cu–Zn–Zr–Al–O catalysts and enhanced the dual-site nature.[27, 42, 43]

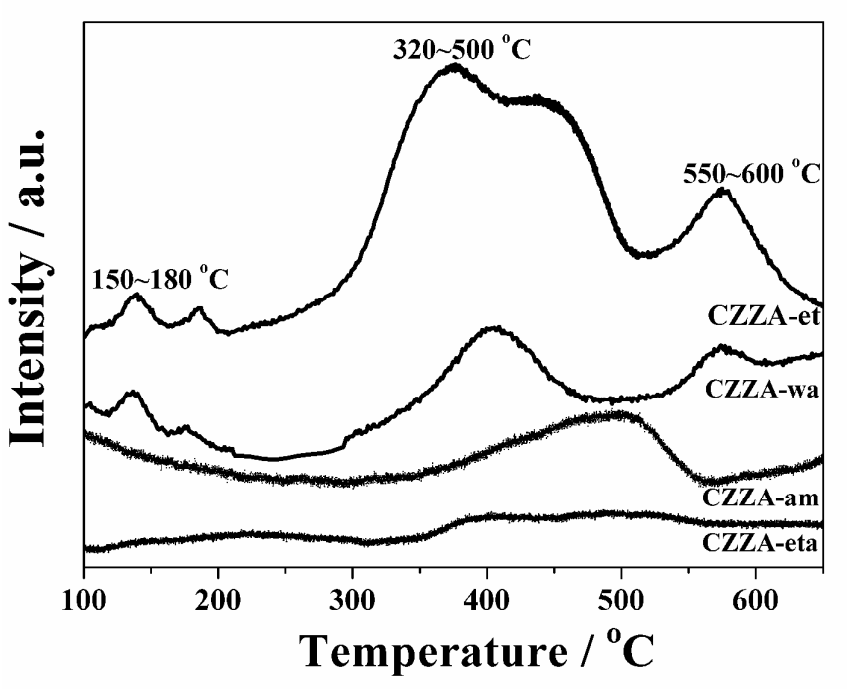

Fig. 6 CO_2-TPD profiles of the reduced CZZA catalysts.

3.6 Effect of solvent on the structure evolution of Cu-Zn-Zr-Al-O catalyst

For amorphous citrate process, the mixture of metal nitrates reacted with CA and formed the hexanuclear complexes. In this process, the CA molecules exist as polymeric skeleton structure containing free carboxyl group and carboxylate groups attached to the metal cation, which acted as a chelating agent and helped in the dispersion of the metal component. For example, coordination of bidentate carboxylate anion on metal ion observed in the composites of copper, alumina, titania, and zirconia with carboxylic acids.[17] The presence of Cu–M_xO_y interaction in the

samples but in different levels was owed to it. However, the CuO in CZZA-am were liable to accumulate partially due to the absence of solvent and thus formed the heterogeneous distribution and agglomerated structure. More discussion about it was as follows.

Solution chemistry of citrate ligands and metal ions was complicated since citrates form complexes containing metal ions of different identity (heteronuclear or mixed-metal complexes). Generally, the polarity of solvent made a great contribution to the citric complexes of Cu-Zn-Zr-Al-O catalysts. In this case, the reduction in hydration/soIvation was related to preorganization or intrinsic basicity of the ligands for complexation of metal ions.[44] Apart from that, we observed that solvents having low dielectric constants (ethanol, 24.3) accelerated the homogeneous complexing process, while solvents having high dielectric constants (water, 80.4) did not have the equivalent effect on the process as ethanol. Compared CZZA-et with CZZA-wa, small copper oxide particles (8~10 nm) and highly dispersed copper species in a strong interaction with the M_xO_y existed in CZZA-et. This could probably be connected with the solvent's capability of stabilizing the polymeric structure of the precursors by building weak/strong hydrogen-bonded networks, which then affected the sintering behavior in the following high-temperature thermal treatment. In addition, the nanostructure was enhanced by solvents of lower polarity.[45] Although the low polarity of ethyl acetate, it contributed little to the catalytic activities of CZZA-eta. Because of the low solubility of metal nitrates and CA in ethyl acetate (≈15 wt.% here), For example, ethyl acetate has negative influence on the catalytic activities of CZZA-eta.

Seriously, the low solubility of CA in ethyl acetate, the dissolution and repolymerization might be inhibited by the non-uniform contact in the heterogeneous suspension, lowering the formation of mixed-metal complexes, as was experimentally observed for CZZA-am without solvent. While water or ethanol was used as solvent, it significantly increased the formation of mixed-metal complexes heightened the dispersion of the Cu species in the M_xO_y matrix by dissolving the components and forming a uniform solution during the process of catalysts' preparing. Regarding above facts, it was obvious that the agglomerated structure of CZZA particles prepared by citrate complex method was induced by the morphology of the precursor gel via using different solvent.[46, 47]

3.7 Performance of CZZA-et catalyst in the reaction of ethanol conversion

As shown in Table 1, the selectivity of ethyl acetate over CZZA-x catalysts were in an order of CZZA-et> CZZA-wa> CZZA-am> CZZA-eta, i.e., decreased in selectivity from 84.9 wt.% to 70.4 wt.%, 58.2 wt.%, and 52.9 wt.%, respectively. This sharp decrease in selectivity can be attributed to the decreased strong basic sites on the CZZA catalysts which catalyzed the bimolecular condensation or dimerization of EtOH to AcOEt.[40] Owing to the decreased dispersion of Cu species and increased particle size of CuO for CZZA-x catalysts, the observed conversion of ethanol decreased with an order of CZZA-et> CZZA-wa> CZZA-am> CZZA-eta as well as selectivity to AcOEt (Table 1).

Among all the catalysts, it was noted that CZZA-et exhibited the best catalytic activities for synthesis of AcOEt (Table 1). Fig. 7a shows the changes in EtOH

conversion, AcOEt selectivity, and yield of AcOEt and H_2 with LHSV at 220 °C and 0.1 MPa over the CZZA-et catalyst. At LHSV= 0.4 mL/(g_{cat}·h), the EtOH conversion was 78.9 wt.%. The ethanol conversion decreased significantly with increasing LHSV. The ethyl acetate selectivity showed a maximum (89.5 wt.%) at LHSV= 0.4 mL/(g_{cat}·h) then decreased slightly with increasing LHSV. It indicated that in the formation of ethyl acetate from ethanol, the stepwise reaction required a prolonged contact time. In the analysis of gaseous products, hydrogen and carbon dioxide were observed: more than 98 mol% of the gaseous products was hydrogen with a small amount of CO_2. The amount of hydrogen produced corresponded to the sum of the derivatives from the dehydrogenation, and the data above had been checked by yield of H_2 and closed to 95 mol% for each experiment. Fig. 7b shows the changes in the selectivity to ethyl acetate and the conversion of the ethanol with reaction pressure. According to Inui[6] and Santacesaria,[8] it was advantageous that the rate of formation of ethyl acetate was accelerated at high pressure by the increase in intermolecular collision frequency. Under an ambient pressure of 0.2 MPa, the selectivity to ethyl acetate was 85.1 wt.% at the temperature of 220 °C and the LHSV of 1.0 mL/(g_{cat}·h). The selectivity to AcOEt greatly increased with increasing reaction pressure, and reached a plateau at around 0.8 MPa (90.1 wt.%) then increased slightly regardless of pressure increasing sharply. In contrast, the observed conversion of ethanol decreased with increasing reaction pressure. Combining the profiles from Fig. 7b, an optimum pressure was about 0.8 MPa in a practical operation because of the relatively high yield of ethyl acetate (56.3 wt.%) without higher pressure.

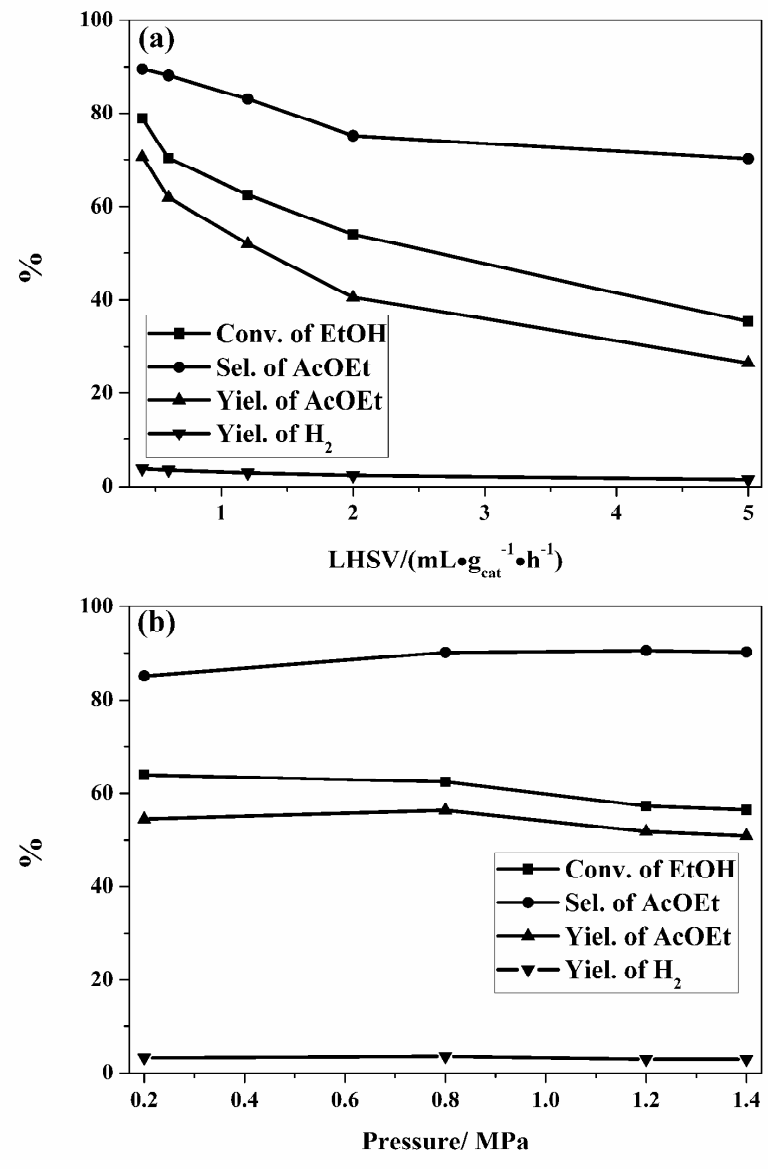

Fig. 7 Changes in conversion of ethanol and selectivity to ethyl acetate over CZZA-et catalyst with (a): LHSV at 220 °C and 0.1 MPa; and with (b): pressure at 220 °C and LHSV= 1.0 mL/(g_{cat}·h).

The reactant of ethanol contains 7 wt.% of water (5 vol.%) was fed over CZZA-et catalysts under varied pressure (Fig. 8a). A selectivity to AcOEt of 80.1 wt.%, which based on 64.4 wt.% conversion of ethanol, was achieved at 220 °C, 0.1 MPa, and LHSV =1.0 mL/(g_{cat}·h). Compared with the reaction of ethanol conversion, the

conversion of hydrous ethanol and formation of the diethyl ether and C4-species were decreased slightly because the aldol addition or hydration reaction retarded by the presence of a little water. However, acetic acid formed together with products of the dehydrogenation of ethanol (data not shown). As the reaction pressure were increased from 0.2 MPa to 0.8 MPa, the selectivity of ethyl acetate increased from 80.1 wt.% to 87.5 wt.%, while the observed conversion of ethanol decreased from 64.4 wt.% to 55.1 wt.%, respectively. It was also found that there was no noticeable improvement of selectivity when the pressure was increased from 0.8 to 1.6 MPa, while the observed conversion of ethanol decreased to 51.5 wt.%. Therefore, the higher pressure would promote competitive adsorption of H_2O and ethanol or acetaldehyde on metallic active sites, which resulted in the decrease of conversion of ethanol.

As we know, water vapor increased the sintering rate of supported metals and leaching of the metal in the reaction system; while carbon deposition was another important reason for catalyst deactivation.[48-50] The stability of the CZZA-et catalyst was evaluated by a test run of 120 h under the following reaction conditions: 220 ^{o}C, atmospheric pressure, and LHSV= 1.0 mL/(g_{cat}·h). As shown in Fig. 8b, at the initial reaction the ethanol conversion was nearly 51.5 wt.% and the selectivity to ethyl acetate was 79.3 wt.%. However, the catalytic activity evidently increased with the reaction time gradually increased during the first 48 h of testing. The ethanol conversion reached to 62.3 wt.%, and the selectivity of ethyl acetate reached to 80.1 wt.% at 48 h. For the first 48 h of testing, the catalytic activity increased because of the instability of the Cu particle after reduction and forming active sites gradually for

ethanol conversion.[48-50] After 48 h, the catalytic activity was stabilized at ethanol conversion of *ca.* 63 wt.% and the selectivity to ethyl acetate was stable at *ca.* 80 wt.%. However, both conversion of ethanol and selectivity to AcOEt remained unchanged, and no deactivation phenomenon was observed for CZZA-et during the 120 h stability test. In addition, mobile oxygen from the M_xO_y support may participate to the oxidation of carbonaceous species at higher temperatures, preventing carbon deposition.[51]

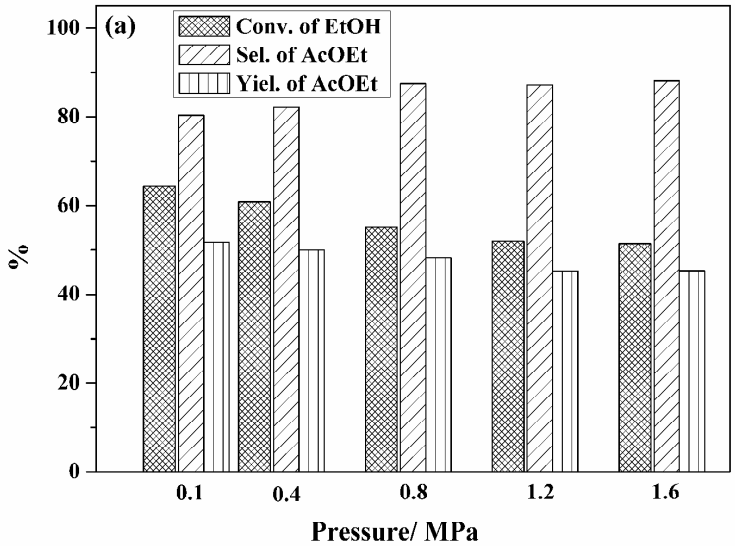

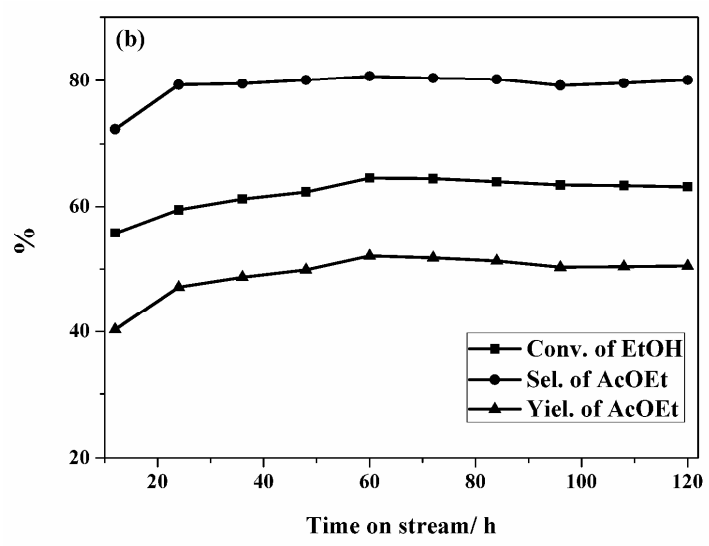

Fig. 8 (a). Changes in conversion of ethanol and selectivity to ethyl acetate with pressure at 220 °C and LHSV= 1.0 mL/(g_{cat}·h) over CZZA-et. (b).Stability evaluation of CZZA-et for dehydrogenative dimerization of ethanol to ethyl acetate at 220 °C and LHSV= 1.0 mL/(g_{cat}·h).

3.8 Applications for the hydrogenation of carbonyl compounds

The hydrogenation of esters is one of the most fundamental and widely employed reactions. As touchstone reactions we have chosen the hydrogenation of diethyl oxalate (DEO) and ethyl acetate, which on copper-based catalysts is known to be critically affected by the amount of metal-active sites.[52] The catalytic performances of the CZZA catalysts prepared by different solvents are listed in Table 2. Steady-state product compositions were obtained after about 36 h on stream and the catalytic activity of all samples remained unchanged after 120 h on stream.

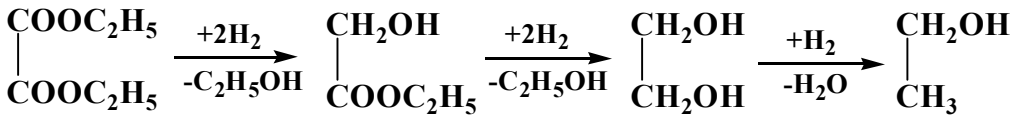

Scheme 1. Reaction pathway for the hydrogenation of DEO to EGT, EG, and ethanol.

It is known that the hydrogenation of DEO proceeds via ethyl glycolate (EGT) to EG (ethylene glycol), while EG can dehydrate further to ethanol (Scheme 1).[53, 54] For pressures above 1.0 MPa, with H_2/ester above 30/1, the formation of EG was favored.[55] The activity and durability of catalyst under severe conditions including low H_2/ester and high space velocity, was tentatively employed in this study. Under the harsh reaction condition specified in Table 2, CZZA-x (x= am, wa, and eta, respectively) showed low activities for hydrogenation of DEO, while the efficiencies were greatly improved when ethanol was used as solvents to prepare the CZZA-et

catalyst. The CZZA-et catalysts which had the highly dispersed Cu also showed better catalytic performances in hydrogenation of AcOEt (Table 2). The results here indicated that the prominent role of ethanol upon preparing Cu-Zn-Zr-Al-O catalyst, could be generalized into hydrogenation of esters, facilitating future work on the CZZA synergy for the hydrogenation of carbonyl groups.

Table 2 Hydrogenation of diethyl oxalate and ethyl acetate over the CZZA-x catalysts.

Catalyst	Conversion [a] of DEO/%	Selectivity[a] /%			Conversion[b] of AcOEt/%	Selectivity[b] /%	
		EG	EtOH	EGT		EtOH	ETA
CZZA-am	51.5	25.6	48.6	19.6	81.2	92.6	1.6
CZZA-wa	63.4	22.1	41.0	26.7	81.6	91.3	2.3
CZZA-et	77.1	55.1	31.6	6.1	95.8	98.3	0.4
CZZA-eta	34.0	15.4	68.5	10.7	79.3	95.9	1.1

[a] Reaction conditions for hydrogenation of DEO: P= 2.4 MPa, T= 240 ^{o}C, H_2/DEO= 25 mol/mol, LHSV= 1.2 mL/(g_{cat}·h). Other byproducts included ethoxyethanol (2-EE), AcOEt, ETA, 1,2-butanediol (1,2-BDO), CO, CO_2, etc.

[b] Reaction conditions for hydrogenation of AcOEt: P= 2.4 MPa, T= 240 ^{o}C, H_2/AcOEt = 25 mol/mol, LHSV= 1 mL/(g_{cat}·h). Other byproducts included AcH, MEK, CROT, PrO, CO, CO_2, ETE, BTE, DEE, and BOL, etc.

3.9 Structure and performance correlation

As can be seen in Table 1, all the samples showed dehydrogenation activity to some extent in conversion of ethanol even CZZA-eta which prepared by employing ethyl acetate as solvent. Still, the catalyst employed ethanol as solvent was distinguished from the other samples because of the existing of quantitatively small CuO particles and abundant Cu-M_xO_y interfaces from XRD, TEM, TPR，H_2-TPD,

CO_2-TPD testing, and so on. However, catalysis was controlled not only by the chemical composition and size of the catalyst used but also by the type of surface sites available at the catalyst surface. As a result, nonlinear relationship between the dispersion of CuO and catalytic activity may be present in the dehydrogenative dimerization of ethanol to ethyl acetate. Moreover, limited by equilibrium conversion of ethanol under the reaction condition employed in this article (*ca.* 74 wt.% conversion of ethanol at 0.1 MPa and 220 °C),[6] it was unobvious for improving of ethanol conversion over the as-prepared Cu-Zn-Zr-Al-O catalyst whatever solvent used. However, the equilibrium of the dehydrogenation of ethanol shifted to synthesis of ethyl acetate, which was achieved by a synergism of metal Cu for dehydrogenation of ethanol and strong basic sites for coupling of ethanol and aldehyde in the CZZA-et. Thus, a high yield to ethyl acetate with increasing conversion of ethanol was obtained. This method was also applied to other systems where high dispersion and small size of Cu species were important, that a series of ethyl esters hydrogenations (*e.g.*, ethyl acetate, and diethyl oxalate), indicating a general promotion of these reactions owed to the highly dispersed Cu species in CZZA-et catalyst.

4. Conclusions

The morphologies and catalytic activities of quaternary Cu-Zn-Zr-Al-O catalysts prepared by citrate-complex method were significantly altered by the utilized of solvent. When a solvent with lower polarity and excellent solubility such as ethanol was employed, the catalyst showed excellent performance in dehydrogenative

dimerization of ethanol to ethyl acetate. When a solvent having higher polarity such as water or low dissolving capacity such as ethyl acetate was used, the catalyst performed poorly in the reaction. Actually, the sample prepared by amorphous citrate process using no solvent also performed poorly in the reaction. Thus, the solute-solvent interaction between ethanol and precursors played an important role in the synthesizing process and the nanostructure was enhanced by lower polarity and prominent solubility of ethanol. Furthermore, the decreased hydration within the alcoholic solution led to a decrease in the size of the metal ions and thus an increased ability to form complex compounds with CA. In fact, the catalyst employed ethanol as solvent was distinguished from the other samples because of the existing of quantitatively small CuO particles and abundant Cu-M_xO_y interfaces from XRD, TEM, and TPR testing. The change in catalytic activities on both samples used was paralleled by a dramatic change in the hydrogen adsorption-desorption properties, as seen from the H_2-TPD profiles. Based on CO_2-TPD, it was verified that the selectivity to ethyl acetate increased with strong basic sites increasing. The promotional roles of solvents can be generalized into hydrogenation of esters (*e.g.*, ethyl acetate and diethyl oxalate), where high dispersion and small size of Cu species were important, indicating a general promotion of these reactions owed to the highly dispersed Cu species. Our study highlighted the design of highly active, selective, and stable Cu catalysts via a simple way, simultaneously solving the low reactivity and deactivation caused by sintering of supported metal catalysts. The results will be useful in the development of supported metal catalysts for a range of dehydrogenation or

hydrogenation reactions and have great implications for practical applications.

Acknowledgement

We would like to thank Mr. Wenbin Zhang and Dr. Yanting Liu for the facilitation in the equipment maintenance, Dr. Shenke Zheng and Zhikai Li for the helpful discussions. This work was supported by the Natural Science Foundation of China (Grant No. 21373254) and PetroChina (Project No. 14-08-05-02).

References

1. C. Gunanathan and D. Milstein, *Science*, 2013, **341**. 249.
2. C. Angelici, B. M. Weckhuysen and P. C. Bruijnincx, *ChemSusChem*, 2013, **6**, 1595-1614.
3. A.L. Wang, H. Xu, J.X. Feng, L.X. Ding, Y.X. Tong and G.R. Li, *J. Am. Chem. Soc.*, 2013, **29**, 10703–10709.
4. J. Llorca, N.S. Homs, J. Sales and P.R.R. de la Piscina, *J. Catal.*, 2002, **209**, 306-317.
5. T.G. Kelly and J.G. Chen, *Green Chem.*, 2014, **16**, 777-784.
6. K. Inui, T. Kurabayashi and S. Sato, *J. Catal.*, 2002, **212**, 207-215.
7. K. Inui, T. Kurabayashi and S. Sato, *Appl. Catal., A*, 2002, **237**, 53-61.
8. E. Santacesaria, G. Carotenuto, R. Tesser and M. Di Serio, *Chem. Eng. J.*, 2012, **179**, 209-220.
9. G. Zeng, T. Chen, L. He, I. Pinnau, Z. Lai and K.W. Huang, *Chem. Eur. J.*, 2012, **18**, 15940-15943.
10. M. Nielsen, H. Junge, A. Kammer and M. Beller, *Angew. Chem. Int. Ed.*, 2012, **51**, 5711-5713.
11. J. Graciani, K. Mudiyanselage, F. Xu, A.E. Baber, J. Evans, S.D. Senanayake, D.J. Stacchiola, P. Liu, J. Hrbek, J.F. Sanz and J.A. Rodriguez, *Science*, 2014, **345**, 546-550.
12. A.G. Sato, D.P. Volanti, I.C. de Freitas, E. Longo and J.M.C. Bueno, *Catal. Commun.*, 2012, **26**, 122-126.
13. I. Freitas, S. Damyanova, D. Oliveira, C. Marques and J. Bueno, *J. Mol. Catal. A*, 2014, **381**, 26-37.
14. A.B. Gaspar, F.G. Barbosa, S. Letichevsky and L.G. Appel, *Appl. Catal., A*, 2010, **380**, 113-117.
15. J.H. Ryu, S.M. Koo, J.W. Yoon, C.S. Lim and K.B. Shim, *Mater. Lett.*, 2006, **60**, 1702-1705.
16. S. Sato, K. Koizumi and F. Nozaki, *J. Catal.*, 1998, **178**, 264-274.
17. S. Samantaray, D.K. Pradhan, G. Hota and B.G. Mishra, *Chem. Eng. J.*, 2012, **193–194**,

1-9.
18. D.W. Kim and S.G. Oh, *Mater. Lett.*, 2005, **59**, 976-980.
19. R.A. Lucky, R. Sui, J.M.H. Lo and P.A. Charpentier, *Cryst. Growth Des.*, 2010, **10**, 1598-1604.
20. J.W. Park and J. S. Shumaker-Parry, *J. Am. Chem. Soc.*, 2014, **136**, 1907-1921.
21. Z.S. Pillai and P.V. Kamat, *J. Phys. Chem. B*, 2003, **108**, 945-951.
22. J. Słoczyński, R. Grabowski, P. Olszewski, A. Kozłowska, J. Stoch, M. Lachowska and J. Skrzypek, *Appl. Catal., A*, 2006, **310**, 127-137.
23. H. Boer, W. Boersma and N. Wagstaff, *Rev. Sci. Instrum.*, 1982, **53**, 349-361.
24. J. Evans, M. Wainwright, A. Bridgewater and D. Young, *Appl. Catal.,* 1983, **7**, 75-83.
25. C. Van Der Grift, A. Wielers, B. Jogh, J. Van Beunum, M. De Boer, M. Versluijs-Helder and J. Geus, *J. Catal.*, 1991, **131**, 178-189.
26. L.R.W. Dai, in: G. Ertl, H. Knozinger, F. Schuth, J. Weitkamp (Eds.),, in *Handbook of Heterogeneous Catalysis*, Wiley-VCH Verlag GmbH, 2008, **vol. 3**, 1st ed., pp. 1064–1077.
27. J. Agrell, H. Birgersson, M. Boutonnet, I. Melián-Cabrera, R.M. Navarro and J.L.G. Fierro, *J. Catal.*, 2003, **219**, 389-403.
28. R.X. Zhou, T.M. Yu, X.Y. Jiang, F. Chen and X.M. Zheng, *Appl. Surf. Sci.* 1999, **148**, 263-270.
29. W.P. Dow, Y.P. Wang and T.J. Huang, *J. Catal.*, 1996, **160**, 155-170.
30. M.F. Luo, Y.J. Zhong, X.X. Yuan and X.M. Zheng, *Appl. Catal., A*, 1997, **162**, 121-131.
31. Q. Yu, L. Qi, T. Tsuru, R. Traylor, D. Rugg, J.W. Morris, M. Asta, D.C. Chrzan and A.M. Minor, *Science*, 2015, **347**, 635-639.
32. A. Sato, D. Volanti, D. Meira, S. Damyanova, E. Longo and J. Bueno, *J. Catal.*, 2013, **307**, 1-17.
33. C.S. Polster, H. Nair and C.D. Baertsch, *J. Catal.*, 2009, **266**, 308-319.
34. F. Arena, K. Barbera, G. Italiano, G. Bonura, L. Spadaro and F. Frusteri, *J. Catal.*, 2007, **249**, 185-194.
35. S. Xia, Z. Yuan, L. Wang, P. Chen and Z. Hou, *Appl. Catal., A*, 2011, **403**, 173-182.
36. F. Arena, G. Italiano, K. Barbera, S. Bordiga, G. Bonura, L. Spadaro and F. Frusteri, *Appl. Catal., A*, 2008, **350**, 16-23.
37. H. Lin, X. Duan, J. Zheng, X. Zheng, P. He, Y. Yuan and Y. Yang, *RSC Adv.*, 2013, **3**, 11782-11789.
38. H. Wilmer, T. Genger and O. Hinrichsen, *J. Catal.*, 2003, **215**, 188-198.
39. Z.Y. Ma, C. Yang, W. Wei, W.H. Li and Y.H. Sun, *J. Mol. Catal. A*, 2005, **227**, 119-124.
40. P.C. Zonetti, J. Celnik, S. Letichevsky, A.B. Gaspar and L.G. Appel, *J. Mol. Catal. A*, 2011, **334**, 29-34.
41. F. Wang, R. Shi, Z.Q. Liu, P.J. Shang, X. Pang, S. Shen, Z. Feng, C. Li and W. Shen, *ACS Catal.*, 2013, **3**, 890-894.
42. S.H. Kang, J.W. Bae, H.S. Kim, G.M. Dhar and K.W. Jun, *Energy Fuels*, 2010, **24**, 804-810.
43. H.W. Lim, M.J. Park, S.H. Kang, H.J. Chae, J.W. Bae and K.W. Jun, *Ind. Eng. Chem. Res.*, 2009, **48**, 10448-10455.
44. A. Martell, R. Hancock and R. Motekaitis, *Coord. Chem. Rev.*, 1994, **133**, 39-65.

45. E. Krupicka, A. Reller and A. Weidenkaff, *Cryst. Eng.*, 2002, **5**, 195-202.
46. R. Takahashi, S. Sato, T. Sodesawa, M. Kawakita and K. Ogura, *J. Phys. Chem. B*, 2000, **104**, 12184-12191.
47. R.T. Wang, L.B. Kong, J.W. Lang, X.W. Wang, S.Q. Fan, Y.C. Luo and L. Kang, *J. Power Sources*, 2012, **217**, 358-363.
48. C. H. Bartholomew, *Appl. Catal., A*, 2001, **212**, 17-60.
49. J.T. Sun, I.S. Metcalfe and M. Sahibzada, *Ind. Eng. Chem. Res.*, 1999, **38**, 3868-3872.
50. R. Hughes, *Chem. Eng. Sci.*, 1989, **44**, 1747-1748.
51. H. Song and U. S. Ozkan, *J. Catal.*, 2009, **261**, 66-74.
52. Y.N. Wang, X. Duan, J. Zheng, H. Lin, Y. Yuan, H. Ariga, S. Takakusagi and K. Asakura, *Catal. Sci. Technol.*, 2012, **2**, 1637-1639.
53. D.J. Thomas, J.T. Wehrli, M.S. Wainwright, D.L. Trimm and N.W. Cant, *Appl. Catal., A*, 1992, **86**, 101-114.
54. Y. Cui, C. Wen, X. Chen and W.L. Dai, *RSC Adv.*, 2014, **4**, 31162-31165.
55. G.H. Xu, Y.C. Li, Z.H. Li and H.J. Wang, *Ind. Eng. Chem. Res.*, 1995, **34**, 2371-2378.